Energy
Advances

rsc.li/energy-advances

ROYAL SOCIETY
OF CHEMISTRY

PAPER
Pin-Yi Zhao, Kwang-Leong Choy *et al.*
Enhanced electrochemical performance by alumina-coated
graphite anodes *via* spray coating

Check for updates

Enhanced electrochemical performance by alumina-coated graphite anodes *via* spray coating†

Pin-Yi Zhao, ID *[abc] Kwang-Leong Choy,*[bc] Yongyi Song,[a] Shudong Zhang[a] and Rui Ma[a]

Lithium-ion batteries (LIBs) are essential for energising portable devices, electric cars, and energy storage systems. Graphite is a frequently utilised anode material; nonetheless, the continual formation of a solid electrolyte interface (SEI) during cycling results in capacity degradation owing to electrolyte depletion. This study tackles this issue by employing alumina coatings on graphite electrodes *via* the spray coating technique, which is cost-effective and scalable. Electrodes with different alumina concentrations (1 wt%, 4 wt%, and 7 wt%) were assessed for electrochemical performance. The 1 wt% alumina-coated electrode demonstrated enhanced cycling stability, with 94.97% capacity retention after 100 cycles, in contrast to 91.74% for the uncoated graphite. The Al_2O_3 coating functions as a preformed SEI, diminishing electrolyte decomposition and improving the cycling performance and rate capability of electrodes, particularly at elevated C-rates. This research illustrates that using spray-coated alumina is an effective technique for enhancing the durability and performance of graphite anodes in lithium-ion batteries, with the potential for extensive applications in energy storage systems.

1. Introduction

Lithium-ion batteries (LIBs) are crucial worldwide for energising portable gadgets utilised in communication, work, and education, while also promoting the development of long-range electric vehicles and the storage of energy from renewable sources, including solar and wind power.[1–3] Graphite is often utilised as a carbon anode in commercial lithium-ion batteries. The electrolyte undergoes decomposition, forming the solid electrolyte interface (SEI) on the graphite anode during the initial lithiation cycles.[4–6] The SEI would protect the electrode and inhibit more electrolyte decomposition. Meanwhile, the SEI will undergo constant renewal during cycling.[7] Continuous electrolyte consumption will exhaust the cell, leading to observable capacity reduction.

Concerted efforts have been undertaken to address this issue. One option involves altering the surface. The coating of Al_2O_3 operates through the mechanism of the "protection effect"[8,9] in which the Al_2O_3 coatings on graphite have been documented to enhance the safety, cycling, and rate performance of cells.[10,11]

Al_2O_3 coatings also serve to safeguard the positive electrode and diminish surface/electrolyte interactions[12,13] or enhance cycling performance by producing $LiPO_2F_2$, a recognised electrolyte additive.[14] Nevertheless, certain processing techniques, such as atomic layer deposition, are highly intricate and expensive, rendering them impractical for large-scale production.[15]

The layer-by-layer (LbL) methodology is an easily implementable and cost-effective method involving the amalgamation of nano-segments to cover diverse areas in various configurations.[16] The LbL approach enables precise control of thickness at the nanoscale level. An exceptional feature of the LbL approach is its capacity to amalgamate organic and inorganic constituents for a thin film, integrating the attributes of each segment.[16] The LbL process presents a promising avenue for attaining a uniform assembly of (1) materials within a narrow size range (100 nm to 1 μm), and (2) highly tailored composites.

Spray coating, as a LbL procedure, is both efficient and cost-effective for covering extensive areas. For example, spray coating may complete a 20-layer sample in about 4 min, but dip coating requires almost 2.5 h.[17] Spray coating entails the application of a liquid substance onto surfaces by techniques such as air spray or electrostatic spray, facilitating uniform coverage and minimising the likelihood of drips and irregularities.[18] This approach is adaptable, and suitable for a range of materials, including paints and specialised coatings. The application of the technique often utilises pressure devices that spray the coating, allowing small

[a] SINOPEC (Dalian) Research Institute of Petroleum and Petrochemicals Co., Ltd., 116045, China

[b] Institute for Materials Discovery, University College London, WC1E 7JE, UK. E-mail: pinyi.zhao.18@ucl.ac.uk, k.choy@ucl.ac.uk

[c] Department of Chemistry, University College London, WC1H 0AJ, UK

† Electronic supplementary information (ESI) available. See DOI: https://doi.org/10.1039/d4ya00582a

particles to cling well to intricate forms and surfaces. Spray coating offers superior regulation of thickness and texture, guaranteeing a uniform surface. Therefore, spray coating is extensively employed in the automotive, aerospace, and construction sectors, showcasing its versatility across diverse substrates and environments.[19]

This study involves the spray coating of graphite electrodes with alumina. Given its versatility and the ability to maintain consistent structure, composition, and thickness control, spray coating is proposed as a technique for electrode coating in batteries. The enhanced electrochemical performance of the as-prepared material is evidenced.

2. Methods

2.1. Calibration

2.1.1. Graphite anodes. Active mass[20]: natural graphite flake (90 wt%), binder: polyvinylidene fluoride (7 wt%), conductive additive: superP (3 wt%), solvent: N-methylpyrrolidone. To prepare the slurry, natural graphite flake (Alfa Aesar), polyvinylidene fluoride (Alfa Aesar), and superP (Timcal) were mixed with N-methylpyrrolidone (Sigma-Aldrich). On a copper foil, the slurry was tape cast (wet thickness: 200 μm).

2.1.2. Al_2O_3 anodes. Active mass: Al_2O_3 (80 wt%), binder: polyvinylidene fluoride (10 wt%), conductive additive: superP (10 wt%), solvent: N-methylpyrrolidone. Al_2O_3 (Sigma-Aldrich), polyvinylidene fluoride (Alfa Aesar) and superP (Timcal) were mixed with N-methylpyrrolidone (Sigma-Aldrich) to get a slurry. The slurry was doctor-bladed (wet thickness: 200 μm) on copper foil. The testing current was 75 mA g^{-1}.

2.2. Electrode coating

Al_2O_3 (<50 nm, Sigma-Aldrich) was dispersed (magnetic stirring overnight) in 10 mL ethanol (absolute ≥99.8%, Fisher Chemical) as 1 wt%, 4 wt%, and 7 wt% spray coating dispersion. The as-prepared graphite (flake, Alfa Aesar) anodes served as the substrate. The substrate temperature was fixed to 80 °C. The airbrush was set to operate at a constant flow rate. The spray coating dispersion was pipetted to a volume of 300 μL. The airbrush and substrate were vertically aligned at a distance of about ~20 cm. The airbrush was pushed back and forth over the substrate at a pace of ~20 cm s^{-1}. The prepared samples were designated G1, G4, and G7, respectively. G0 designated graphite anodes which were not coated.

2.3. Material characterisations

Energy-dispersive X-ray spectrometry (Oxford Instruments, UK) was applied to map the elements. The X-ray diffraction (XRD) system (X'Pert PRO, PANalytical, Netherlands) was operated at 40 kV and 40 mA at a scan rate of 0.2° s^{-1} and 2 theta within the range of 10° to 75°. Images from scanning electron microscopy (SEM) were obtained from the ZEISS EVO LS15.

2.4. Electrochemistry

CR2032 coin cells were assembled. The electrolyte (LP30) from Sigma-Aldrich was 1.0 M $LiPF_6$ in ethylene carbonate (EC) and dimethyl carbonate (DMC), with EC/DMC = 50/50 (v/v). The measurements were performed in a two-electrode setup. Galvanostatic discharge/charge (GDC) measurements were carried out on a test system (4300M, Maccor, USA) at room temperature within [0.005, 2] V. Galvanostatic electrochemical impedance spectroscopy (EIS) was performed with an alternating current of 0.0001 A within 10^6 Hz to 0.01 Hz at room temperature (~21.0 °C) on the Gamry (Interface 1010E, Gamry, USA).

3. Results and discussion

Table 1 presents comprehensive characteristics of the constructed cells. Fig. 1a illustrates the initial four GDC cycles of graphite anodes. The specific capacity during the initial cycle (charging) is 360 mAh g^{-1}. CE increases from 81.47% in the first cycle to 97.39% in the second cycle, 98.31% in the third cycle, and 98.66% in the fourth cycle. The staging phenomenon is indexed from ref. 21 and shown in Fig. 1b.

Fig. 1c illustrates that the electrode exhibits negligible capacity attributable to Al_2O_3, indicating that Al_2O_3 should be considered inert mass that does not enhance the specific capacity.

Coating powders directly is inadvisable because the insulating layer on the particles impedes the diffusion of Li^+ ions and electron transport. Nonetheless, directly coating electrodes facilitates the establishment of a conductive pathway among particles. A uniform electrode surface coating is essential for attaining optimal electrochemical performance.[8]

Fig. 2a depicts an illustration of the coated electrode where substrate, electrode and coating are shown. Fig. S1 (ESI†) shows the SEM images of G0, G1, G4, and G7. No noticed variations among images are observed. Fig. 2b displays the XRD spectra of G0, G1, G4, G7, and Al_2O_3 powder. Fig. 2b is shown on this scale due to the remarkable intensity of the graphite (002) peak. No discernible alterations in the graphite crystal structure are seen in any of the four samples, suggesting that the spray coating process does not influence the crystal structure of the core material. The peaks at 36° and 67° correspond to Al_2O_3 (104) and (110), respectively.[15] No significant difference in the XRD patterns of G4 and G7 is detected. Owing to the low mass ratio and amorphous characteristics of Al_2O_3, no discernible peaks of Al_2O_3 in the sample G1 can be seen.[10]

Fig. 3 illustrates the elemental mapping of carbon, aluminium, and oxygen in the as-prepared G1, G4, and G7 samples.

Table 1 Parameters of the cell

| Component	Feature	Value
Graphite electrode	Areal capacity (mAh cm^{-2})	0.807
	Mass loading (mg cm^{-2})	2.17
Lithium metal	Thickness (μm)	250
Current collector	Thickness (mm)	0.010–0.012
Electrolyte	Composition	LP30
	Electrolyte amount (drops)	14
Separator: glass fibre	Thickness (mm)	0.556
Testing conditions	Testing temperature (°C)	25
	Minimum resting time (h)	12
	Potential range (V)	0.005–2
	Current density (mA cm^{-2})	0.0807
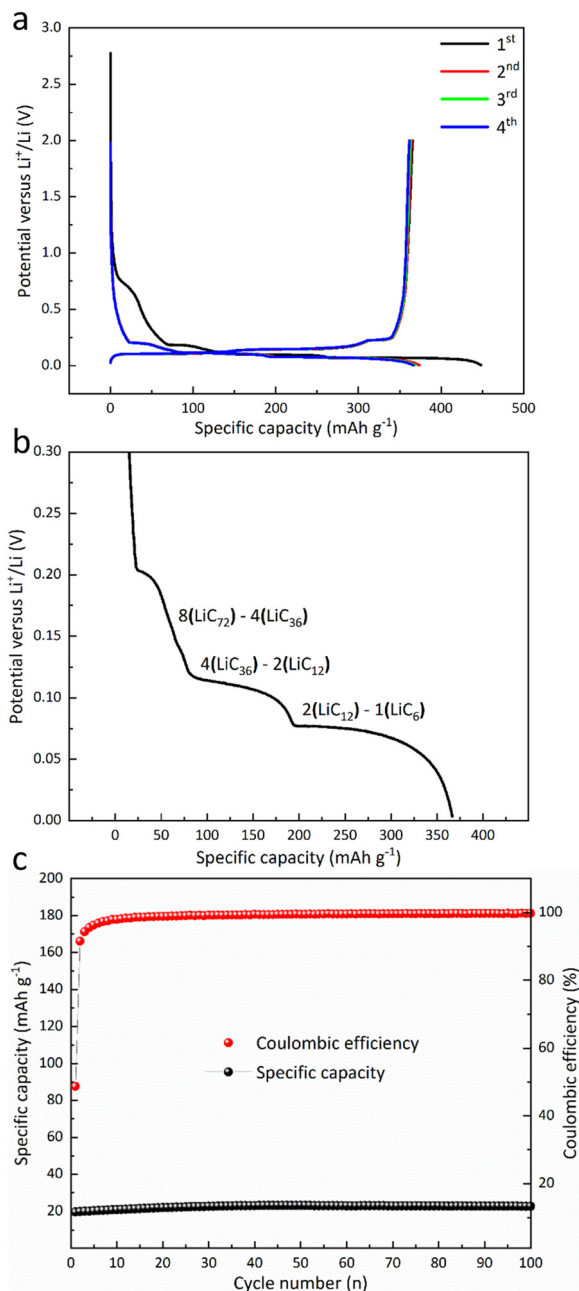
Fig. 1 (a) GDC curves of graphite anodes (cycles 1–4), (b) staging phenomenon (staging information from ref. 21), and (c) cycling performance of the raw material Al_2O_3 at 75 mA g^{-1}.
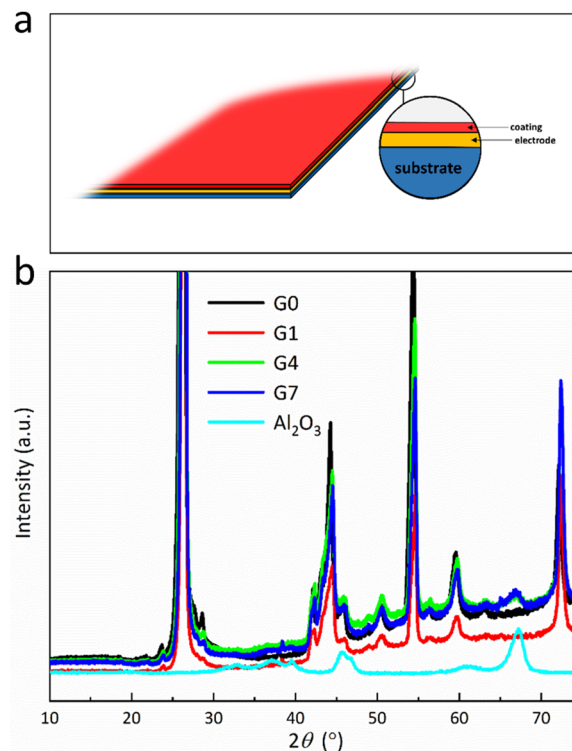

Fig. 2 (a) Illustration of the obtained materials, and (b) XRD spectra of the samples and the raw Al_2O_3 powder.
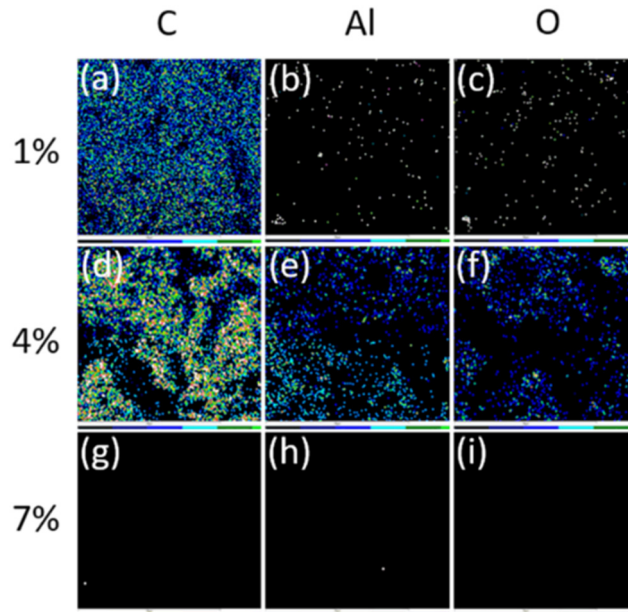

Fig. 3 Energy-dispersive X-ray spectrometry (EDS) elemental mapping of carbon, aluminium, and oxygen in G1, G4, and G7, respectively: (a) C in G1, (b) Al in G1, (c) O in G1, (d) C in G4, (e) Al in G4, (f) O in G4, (g) C in G7, (h) Al in G7, (i) O in G7.

It is demonstrated that all elements are detected when the weight proportion of components increases (G1 to G4). Nonetheless, a negligible signal in G7 may be affected by the coating bulk and electrical conductivity. Note that carbon mapping should be excluded as it is outside the purview of EDS.[22]

Fig. 4a illustrates the second-cycle GDC profile. As the mass ratio of Al_2O_3 coating increases, the specific charge capacity diminishes. The rationale for this is that the Al_2O_3 coating provides insufficient electrical conductivity, adversely affecting the specific capacity of lithium-ion batteries despite assertions of strong ionic conductivity.[23] The initial coulombic efficiencies of the G0, G1, G4, and G7 are 81.5%, 82%, 82.3%, and 82.4%, respectively. The initial coulombic efficiency is positively related with the increases of the Al_2O_3 coating amount since
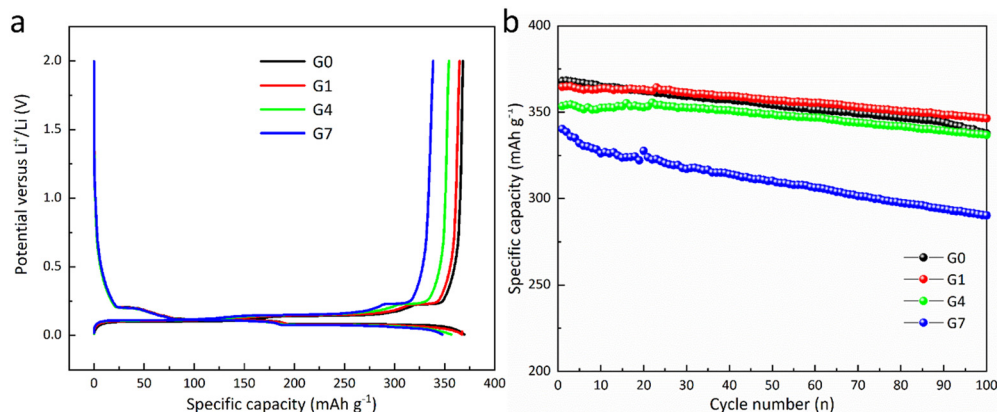
Fig. 4 (a) GDC curves for the second cycle at 0.1C within [0.005, 2] V, and (b) cycling stability of the samples at 0.1C within [0.005, 2] V.

Al_2O_3 coating may reduce excess lithium-ion consumption and inhibit adverse effects.[10]

Fig. 4b illustrates the cycling stability of G1, G4, and G7 in comparison to G0 at 0.1C within [0.005, 2] V. G0, G1, G4, and G7 have specific charge capacities and capacity retention of 338 mAh g^{-1} (91.74%), 346 mAh g^{-1} (94.97%), 337 mAh g^{-1} (95.23%), and 290 mAh g^{-1} (85.29%), respectively. G1 and G4 exhibit superior capacity retention compared to G0, potentially attributable to the Al_2O_3 as the preformed SEI and the robust ionic conductivity derived from the stable Li–Al–O glass phase.[23] Due to the limited performance of the G7, it is not considered in the following steps.

Fig. 5a illustrates the rate capacity of G0, G1, and G4 over different C-rates (0.1C–10C). It is demonstrated that when the C-rate surpasses 1C, G1 exhibits slightly better performance compared to G0 and G4. A slender layer with little ohmic polarisation yields a high specific capacity at low C-rates. However, at elevated C-rates, SEI regeneration leads to a comparatively diminished specific capacity.[15] G1 operates at peak efficiency due to the coating functioning effectively as a preformed SEI, which reduces the loss of Li$^+$ ions during SEI regeneration throughout cycling.

Fig. 5b displays the EIS spectra of G0, G1, and G4. Throughout the whole frequency spectrum, Nyquist plots exhibit three overlapping semicircles. The semicircles at high frequency correspond to the R_{ct} of lithium-ion batteries. The low-frequency line pertains to the Z_w. The R_{ct} rises, moving from G0 ($\sim$6.5 Ω), to G1 ($\sim$7.5 Ω), to G4 ($\sim$8.5 Ω) when the weight fraction of Al_2O_3 is increased.

A performance comparison between this study and existing literature is presented in Table 2. This work presents slightly better cycle retention. However, it is important to acknowledge that the electrochemical performance values are often not precisely comparable across different studies due to varying conditions, including fabrication methods, operational duration, binders, electrolytes, characterisations, and the limited information available. Standardisation initiatives have been undertaken within the battery sector,[24–26] though no consensus has been reached yet.
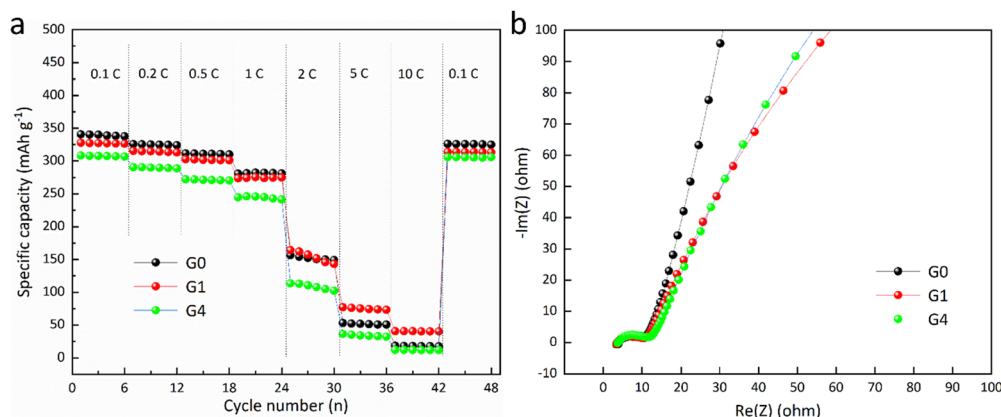
Table 2 Comparison of the fabrication methods and electrochemical performances

Fabrication method	Current density and potential	Cycles	Retention (%)	Ref.
Sol–gel	1C, 3–4.35 V	200	84.95	10
Sol–gel	400 mA g^{-1}, 0.005–2 V	100	94	11
Spray coating	0.1C, 0.005–2 V	100	94.97	This work

Fig. 5 (a) Rate capacity at various C-rates (0.1C–10C) of G0, G1, and G4, and (b) EIS spectra of G0, G1, and G4.

4. Conclusions

In summary, Al_2O_3-coated graphite anodes have been effectively produced by spray coating. The anode coated with 1 wt% Al_2O_3 enhances cycling stability and improves rate performance. Using spray-coated alumina through the layer-by-layer method is a viable approach to improve the efficiency and durability of graphite anodes in lithium-ion batteries. This method efficiently reduces electrolyte breakdown and enhances the integrity of the SEI, addressing capacity loss while promoting safety and efficiency during cycling. The scalability and cost-efficiency of spray coating render it an appealing choice for mass manufacturing, possibly facilitating substantial progress in battery technology and enabling the development of more dependable and high-performance energy storage options.

Data availability

Data will be available upon request to the authors.

Conflicts of interest

The authors declare that they have no known conflicting financial interests or personal relationships that would seem to have influenced the work presented in this work.

Acknowledgements

References

1 A. Manthiram and J. B. Goodenough, *Nat. Energy*, 2021, **6**(3), 323.

2 M. S. Whittingham and J. Xiao, *MRS Bull.*, 2023, **48**(11), 1118–1124.

3 A. Yoshino, *Bull. Chem. Soc. Jpn.*, 2022, **95**(1), 195–197.

4 E. Peled, *J. Electrochem. Soc.*, 1979, **126**(12), 2047–2051.

5 D. Aurbach, *et al.*, *J. Electrochem. Soc.*, 1996, **143**(12), 3809–3820.

6 J. B. Goodenough and K.-S. Park, *J. Am. Chem. Soc.*, 2013, **135**(4), 1167–1176.

7 S. J. An, *et al.*, *Carbon*, 2016, **105**, 52–76.

8 Y. S. Jung, *et al.*, *Adv. Mater.*, 2010, **22**(19), 2172–2176.

9 Y. He, *et al.*, *Adv. Mater.*, 2011, **23**(42), 4938–4941.

10 T. Xu, *et al.*, *Chin. J. Chem.*, 2019, **37**(4), 342–346.

11 D. S. Kim, *et al.*, *J. Power Sources*, 2019, **422**, 18–24.

12 Y. S. Jung, *et al.*, *J. Electrochem. Soc.*, 2010, **157**(1), A75–A81.

13 C. Li, *et al.*, *Electrochim. Acta*, 2006, **51**(19), 3872–3883.

14 D. S. Hall, *et al.*, *ACS Appl. Mater. Interfaces*, 2019, **11**(15), 14095–14100.

15 T. Feng, *et al.*, *ACS Appl. Mater. Interfaces*, 2016, **8**(10), 6512–6519.

16 P. T. Hammond, *AIChE J.*, 2011, **57**(11), 2928–2940.

17 A. Izquierdo, *et al.*, *Langmuir*, 2005, **21**(16), 7558–7567.

18 A. Reale, *et al.*, *Energy Technol.*, 2015, **3**(4), 385–406.

19 U. P. Gaur and E. Kamari, *J. Therm. Spray Eng.*, 2024, **4**, 106–114.

20 K. Ueno, *et al.*, *J. Electrochem. Soc.*, 2017, **164**(1), A6088–A6094.

21 J. Dahn, *Phys. Rev. B: Condens. Matter Mater. Phys.*, 1991, **44**(17), 9170.

22 Y. Leng, *Materials characterization: introduction to microscopic and spectroscopic methods*, John Wiley & Sons, 2009.

23 Y. Liu, *et al.*, *Nano Lett.*, 2011, **11**(10), 4188–4194.

24 B. R. Long, *et al.*, *J. Electrochem. Soc.*, 2016, **163**(14), A2999–A3009.

25 S. J. An, *et al.*, *J. Electrochem. Soc.*, 2017, **164**(6), A1195–A1202.

26 J. Li, *et al.*, *J. Pharm. Sci.*, 2020, **452**, 227824.